Inorg. Chem. **2007**, *46*, 5237–5242

Remarkable Changes in the Optical Properties of CeO_2 Nanocrystals Induced by Lanthanide Ions Doping

Zhenling Wang,[†,‡] Zewei Quan,[†] and Jun Lin*[,†]

Key Laboratory of Rare Earth Chemistry and Physics, Changchun Institute of Applied Chemistry, Chinese Academy of Sciences, Changchun 130022, P. R. China, and Department of Chemistry, Zhoukou Normal University, Zhoukou 466000, P. R. China

Received January 25, 2007

Highly uniform and well-dispersed CeO_2 and CeO_2:Eu^{3+} (Sm^{3+}, Tb^{3+}) nanocrystals were prepared by a nonhydrolytic solution route and characterized by X-ray diffraction (XRD), transmission electron microscopy (TEM), X-ray photoelectron spectra (XPS), UV/vis absorption, and photoluminescence (PL) spectra, respectively. The result of XRD indicates that the CeO_2 nanocrystals are well crystallized with a cubic structure. The TEM images illustrate that the average size of CeO_2 nanocrystals is about 3.5 nm in diameter. The absorption spectrum of CeO_2:Eu^{3+} nanocrystals exhibits red-shifting with respect to that of the undoped CeO_2 nanocrystals. Under the excitation of 440 nm (or 426 nm) light, the colloidal solution of the undoped CeO_2 nanocrystals shows a very weak emission band with a maximum at 501 nm, which is remarkably enhanced by doping additional lanthanide ions (Eu^{3+}, Tb^{3+}, Sm^{3+}) in the CeO_2 nanocrystals. The emission band is not due to the characteristic emission of the lanthanide ions but might arise from the oxygen vacancy which is introduced in the fluorite lattice of the CeO_2 nanocrystals to compensate the effective negative charge associated with the trivalent ions.

Introduction

Rare-earth oxides with different nanostructures are of great importance because of their applications in high-performance luminescent devices, biological labeling, magnets, and catalysts based on the electronic, optical, and chemical characteristics arising from their 4f electrons.[1−8] Compared with the other nanostructured lanthanide oxides, CeO_2 nanocrystals have been widely investigated as important functional materials.[6−17] CeO_2 nanoparticles can be used as three-way catalysts (TWC) for exhaust gas treatment from automobiles, oxygen ion conductors in solid oxide fuel cells, polishing agents for the chemical mechanical planarization (CMP) process, gate oxides in metal oxide semiconductor devices, and ultraviolet (UV) blocking materials in UV shielding, respectively.[6−10] Nanostructured CeO_2 has been prepared by various methods such as forced hydrolysis,[11] the microemulsion method,[12] solvothermal synthesis,[6a,8] the two-stage precipitation process,[13] nonhydrolytic sol−gel synthesis,[6b,7] solid-state reactions,[14] mechanochemical reactions,[15] sonochemical synthesis,[16,17] microwave irradiation,[18] and so on.

* To whom correspondence should be addressed. E-mail: jlin@ciac.jl.cn.
† Chinese Academy of Sciences.
‡ Zhoukou Normal University.

(1) (a) Wu, G. S.; Zhang, L. D.; Cheng, B. C.; Xie, T.; Yuan, X. Y. *J. Am. Chem. Soc.* **2004**, *126*, 5976. (b) Yu, M.; Lin, J.; Fu, J.; Zhang, H. J.; Han, Y. C. *J. Mater. Chem.* **2003**, *13*, 1413.
(2) Wakefield, G.; Keron, H. A.; Dobson, P. J.; Hutchison, J. L. *J. Colloid Interface Sci.* **1999**, *215*, 179.
(3) Wang, H. Z.; Uehara, M.; Nakamura, H.; Miyazaki, M.; Maeda, H. *Adv. Mater.* **2005**, *17*, 2506.
(4) Cao, Y. C. *J. Am. Chem. Soc.* **2004**, *126*, 7456.
(5) Feldmann, C. *Adv. Funct. Mater.* **2003**, *13*, 101.
(6) (a) Zhang, Y. W.; Si, R.; Liao, C. S.; Yan, C. H.; Xiao, C. X.; Kou, Y. *J. Phys. Chem. B* **2003**, *107*, 10159. (b) Si, R.; Zhang, Y. W.; You, L. P.; Yan, C. H. *Angew. Chem., Int. Ed.* **2005**, *44*, 3256.
(7) Yu, T.; Joo, J.; Park, Y. I.; Hyeon, T. *Angew. Chem., Int. Ed.* **2005**, *44*, 7411.
(8) Wang, Z. L.; Feng, X. D. *J. Phys. Chem. B* **2003**, *107*, 13563.
(9) Miki, T.; Ogawa, T.; Haneda, M.; Kakuta, N.; Ueno, A.; Tateishi, S.; Matsuura, S.; Sato, M. *J. Phys. Chem.* **1990**, *94*, 6464.
(10) Tsunekawa, S.; Fukuda, T.; Kasuya, A. *J. Appl. Phys.* **2000**, *87*, 1318.
(11) Hsu, W. P.; Rönnquist, L.; Matijević, E. *Langmuir* **1988**, *4*, 31.
(12) Masui, T.; Fujiwara, K.; Machida, K.; Adachi, G.; Sakata, T.; Mori, H. *Chem. Mater.* **1997**, *9*, 2197.
(13) Djurièiæ, B.; Pickering, S. *J. Eur. Ceram. Soc.* **1999**, *19*, 1925.
(14) Li, F.; Yu, X. H.; Pan, H. J.; Wang, M. L.; Xin, X. Q. *Solid State Sci.* **2000**, *2*, 767.
(15) Li, Y. X.; Zhou, X. Z.; Wang, Y.; You, X. Z. *Mater. Lett.* **2003**, *58*, 245.
(16) Xia, B.; Lenggoro, I. W.; Okuyama, K. *J. Mater. Chem.* **2001**, *11*, 2925.
(17) Yin, L. X.; Wang, Y. Q.; Pang, G. S.; Koltypin, Y.; Gedanken, A. *J. Colloid Interface Sci.* **2002**, *246*, 78.

10.1021/ic0701256 CCC: $37.00
Published on Web 05/23/2007

However, it is difficult to synthesize highly uniform and well-dispersed CeO_2 nanocrystals on the basis of the following reasons. First, it is not easy to choose the appropriate precursor complexes and the crystalline temperatures for rare-earth oxides are relatively high. Second, the agglomeration of nanopcrystals is very common because the nanocrystals tend to decrease the exposed surface to lower the surface energy. Hence the literature on the synthesis of highly uniform and well-dispersed CeO_2 nanocrystals is limited.[6b,7,12,19a] On the other hand, most of the investigations on CeO_2 nanocrystals with particle size less than 10 nm were focused on the lattice relaxation effect,[19] ultraviolet absorption properties, and catalytic activity.[6a,10,12,19a,j] So far only a few researchers have reported lanthanide ion-doped CeO_2 systems together with their luminescent properties.[20] To the best of our knowledge, the synthesis of uniform and well-dispersed lanthanide ion-doped (Eu^{3+}, Tb^{3+}, Sm^{3+}) CeO_2 nanocrystals and their luminescent properties have not been reported. In this paper, we synthesized the CeO_2 nanocrystals doped and undoped with other lanthanide ions (Eu^{3+}, Tb^{3+}, Sm^{3+}) via a high-boiling-point solvent process and reported their optical properties. It is interesting to note that the undoped CeO_2 nanocrystals show a very weak emission band peaking at 501 nm, which is remarkably enhanced by doping additional lanthanide ions (Eu^{3+}, Tb^{3+}, Sm^{3+}) in the CeO_2 nanocrystals. The greatly increased emission band of CeO_2:Eu^{3+} (Tb^{3+}, Sm^{3+}) nanocrystals (located at 500 nm) is not attributed to the characteristic emission of the lanthanide ions (Eu^{3+}, Tb^{3+}, Sm^{3+}) but may arise from the presence of an oxygen vacancy in the lattices of CeO_2 nanocrystals.

Experimental Section

Synthesis of CeO_2 Nanocrystals Undoped and Doped with Lanthanide Ions. The CeO_2-based nanocrystals were prepared by the nonhydrolytic solvent method in the hexadecane−oleylamine−oleic acid system.[21] Cerium(III) acetate hydrate (99.999%, Aldrich), hexadecane (≥98%, Fluka), oleyamine (70%, Aldrich), oleic acid (analytical reagent, AR, Beijing Chemical Reagent Co.), and sodium hydroxide (≥96.0%, AR, Beijing Chemical Reagent Co.) were used as received for starting materials. $Eu(CH_3COO)_3$, $Sm(CH_3COO)_3$, and $Tb(CH_3COO)_3$, were prepared by dissolving the corresponding oxides in acetic acid, and the water in the solutions was distilled off by heating. Typically, 0.4 mmol of cerium(III) acetate hydrate or the stoichiometric amounts of the rare earth acetates (the doping concentrations of Eu^{3+}, Tb^{3+}, and Sm^{3+} are 5 mol % of that of Ce^{3+}), 0.55 mL of oleyamine, and 0.60 mL of oleic acid were mixed with 7.0 mL of hexadecane in a three-neck flask equipped with a condenser. The system was pumped under vacuum at room temperature for 15 min and then heated at 90 °C for 1 h, to form a clear light yellow solution. At 90 °C, 0.06 g of NaOH was added to the clear solution and the system was pumped again under vacuum to remove the minimum water. Then, the solution was heated to 280 °C and remained for 3 h under agitation and argon protection. The solution changed gradually to a brown turbid slurry with the increase of reaction time. These turbid slurries were cooled to room temperature and then isolated and washed by adding a sufficient amount of ethanol and separating by centrifugation. The yielded precipitate can be well dispersed in hexane to form a transparent colloidal solution.

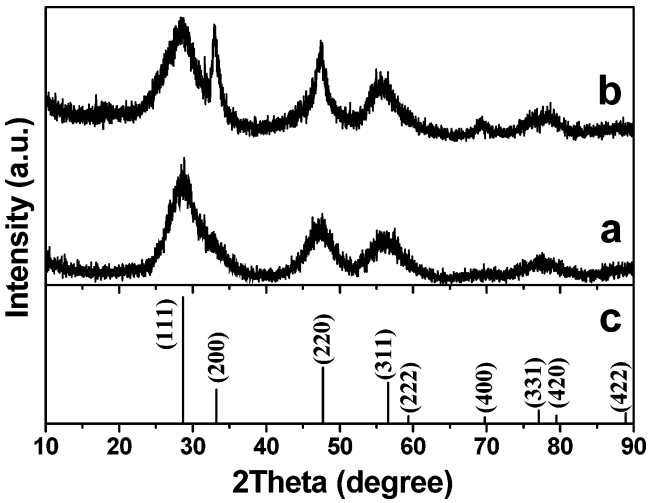

Figure 1. XRD patterns of CeO_2 (a), CeO_2: Eu^{3+} (b) nanocrystals, and the standard data for bulk CeO_2 (c; JCPDS Card No. 75-0076).

Characterization. X-ray diffraction (XRD) was carried out on a Rigaku-Dmax 2500 diffractometer with Cu Kα radiation (λ = 0.154 05 nm). TEM images were obtained using a JEOL 2010 transmission electron microscope operating at 200 kV. Samples for TEM were prepared by depositing a drop of the colloidal solution onto a carbon-coated copper grid. The excess liquid was wiped out with filter paper, and the grid was dried in air. The particle size distribution histograms were measured with dynamic light scattering (DLS) using a ZETASIZER 1000 HS_A instrument. The UV/vis absorption spectra were measured on a TU-1901 spectrophotometer. The X-ray photoelectron spectra (XPS) were taken on a VG ESCALAB MK II electron spectrometer using Mg Kα (1253.6 eV) as the exciting source. The excitation and emission spectra were taken on an F-4500 spectrophotometer equipped with a 150 W xenon lamp as the excitation source. All the measurements were performed at room temperature.

Results and Discussion

Phase Structure and Morphology of the Nanocrystals. XRD. Figure 1 shows the XRD patterns of CeO_2 (a), CeO_2: Eu^{3+} (b) nanocrystals, and the standard data for bulk CeO_2 (c). The results of XRD indicate that the CeO_2 nanocrystals are well-crystallized and the patterns are in good agreement with a cubic structure (space group, $Fm\bar{3}m$ (No. 225); cell, 0.5389 × 0.5389 × 0.5389 nm^3 and $\alpha = \beta = \gamma = 90°$)

(18) Liao, X. H.; Zhu, J. M.; Zhu, J. J.; Xu, J. Z.; Chen, H. Y. *Chem. Commun.* **2001**, 937.
(19) (a) Tsunekawa, S.; Sivamohan, R.; Ohsuna, T.; Kasuya, A.; Takahashi, H.; Tohji, K. *Mater. Sci. Forum* **1999**, 315−317, 439. (b) Tsunekawa, S.; Sahara, R.; Kawazoe, Y.; Ishikawa, K. *Appl. Surf. Sci.* **1999**, *152*, 53. (c) Tsunekawa, S.; Ishikawa, K.; Li, Z. Q.; Kawazoe, Y.; Kasuya, A. *Phys. Rev. Lett.* **2000**, *85*, 3440. (d) Tsunekawa, S.; Ito, S.; Kawazoe, Y. *Appl. Phys. Lett.* **2004**, *85*, 3845. (e) Tsunekawa, S.; Wang, J.-T.; Kawazoe, Y. *J. Alloys Compd.* **2006**, 408−412, 1145. (f) Zhou, X.-D.; Huebner, W. *Appl. Phys. Lett.* **2001**, *79*, 3512. (g) Zhang, F.; Chan, S.-W.; Spanier, J. E.; Apak, E.; Jin, Q.; Robinson, R. D.; Herman, I. P. *Appl. Phys. Lett.* **2002**, *80*, 127. (h) Wu, L. J.; Wiesmann, H. J.; Moodenbaugh, A. R.; Klie, R. F.; Zhu, Y.; Welch, D. O.; Suenaga, M. *Phys. Rev. B* **2004**, *69*, 125415. (i) Zhang, F.; Jin, Q.; Chan, S.-W. *J. Appl. Phys.* **2004**, *95*, 4319. (j) Tsunekawa, S.; Wang, J.-T.; Kawazoe, Y.; Kasuya, A. *J. Appl. Phys.* **2003**, *94*, 3654.
(20) (a) Linares, R. C. *J. Opt. Soc. Am.* **1966**, *56*, 1700. (b) Yugami, H.; Nakajima, A.; Ishigame, M.; Suemoto, T. *Phys. Rev. B* **1991**, *44*, 4862. (c) Fujihara, S.; Oikawa, M. *J. Appl. Phys.* **2004**, *95*, 8002.
(21) (a) Liu, Q.; Lu, W.; Ma, A.; Tang, J.; Lin, J.; Fang, J. *J. Am. Chem. Soc.* **2005**, *127*, 5276. (b) Gu, H.; Soucek, M. D. *Chem. Mater.* **2007**, *19*, 1103.

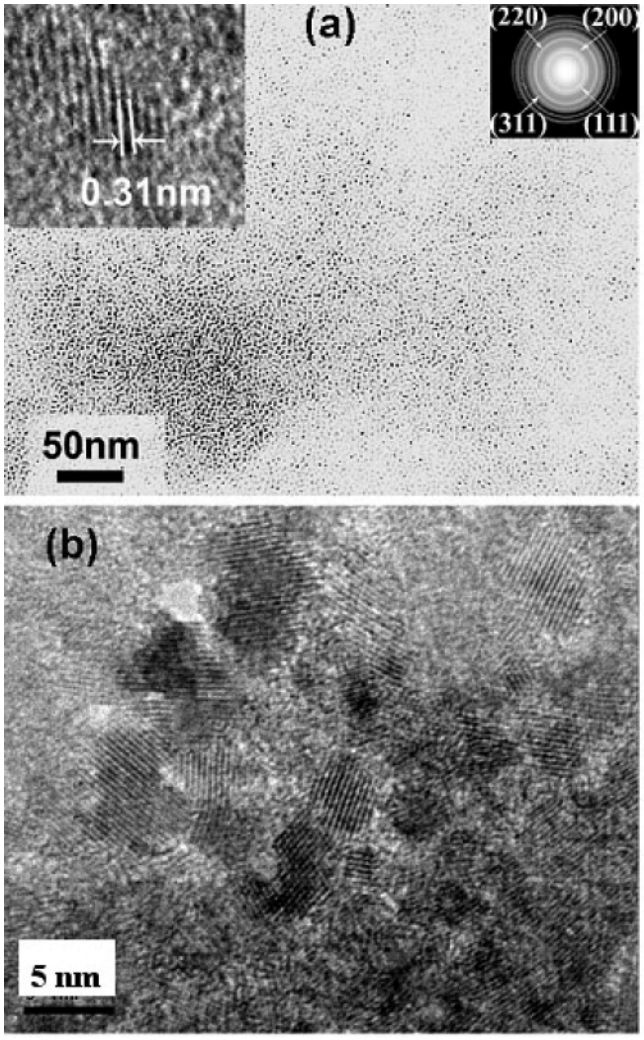

Figure 2. TEM micrograph of CeO_2 nanocrystals (a; insets are the high-resolution TEM image and a selected area electron diffraction pattern, SAED) and the HRTEM image of CeO_2: Eu^{3+} nanocrystals (b).

known from bulk CeO_2 (JCPDS Card No. 75-0076). According to the Scherrer equation, the strongest peak (111) at $2\theta = 28.7°$ and the peak (220) at $2\theta = 47.1°$ were used to calculate the average crystallite size of CeO_2 nanocrystals, determined to be around 2.0 nm. The calculated cell parameter (a) is equal to 0.5426 nm, a little larger than that of bulk CeO_2 (0.5389 nm, JCPDS Card No. 75-0076). This is due to the lattice expansion effect resulting from increased oxygen vacancies and Ce^{3+} ions with decreasing particle size.[19b,c,f−h] When CeO_2 nanocrystals were doped with Eu^{3+} ions, all diffraction peaks can still be indexed to the cubic structure of CeO_2 phase, as shown in Figure 1b. Compared with the undoped CeO_2 nanocrystals, the peak (200) at $2\theta = 33.0°$ was present in the XRD patterns of the doped sample, which may be due to the anisotropic growth induced by the doping ions. The average crystal size of CeO_2:Eu^{3+} nanocrystals estimated by the Scherrer equation increased to 2.6 nm, and the calculated cell parameter values decrease slightly (0.5394 nm).

TEM. Figure 2a shows a typical TEM image of CeO_2 nanocrystals. From the TEM image it can be seen that the mean diameter of CeO_2 nanocrystals is about 3.5 nm, which

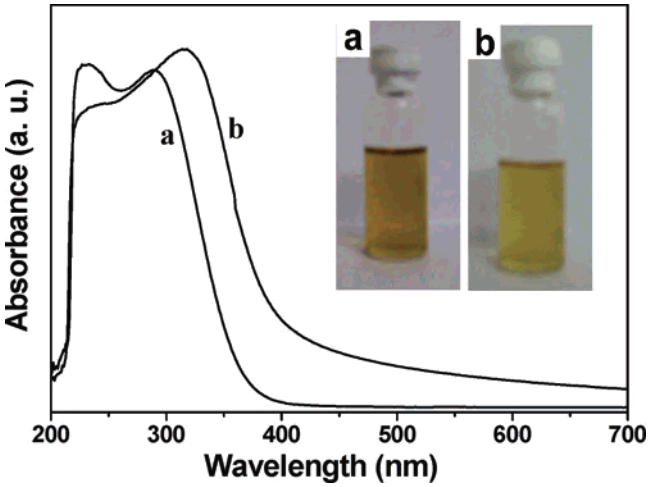

Figure 3. UV/vis absorption spectra of CeO_2 (a) and CeO_2:Eu^{3+} (b) nanocrystals solution. Insets are the photographs of these two samples (in hexane solution).

is larger than that (2.0 nm) calculated from the Scherrer equation. This demonstrates that the CeO_2 nanocrystals are of polycrystalline nature. The high-resolution TEM image (left inset) displays lattice fringes for nanocrystals, indicating that these CeO_2 nanocrystals possess high crystallinity. The interplanar spacing of the CeO_2 nanocrystals is about 0.31 nm, which is identical with the (111) facet distance of bulk CeO_2 phase. The selected area electron diffraction (SAED) patterns (right inset) are consistent with a cubic structure of CeO_2 with strong ring patterns due to (111), (200), (220), and (311) planes, in good agreement with the XRD result. The particle size distribution histogram of CeO_2 nanocrystals measured with the dynamic light scattering technique is shown in Figure S-1 (Supporting Information). It can be seen that the size distribution of CeO_2 nanocrystals is narrow with an average particle size of 3.8 nm, in agreement with the result observed by TEM image. As for CeO_2:Eu^{3+} nanocrystals, the doping of Eu^{3+} ions resulted in the increase of crystallinity, the presence of an irregular morphology, and a little larger particle size compared with the undoped nanocrystals, as shown in the typical high-resolution TEM image of CeO_2:Eu^{3+} nanocrystals (Figure 2b, bottom). This result is basically consistent with that observed by XRD data.

Optical Properties. UV/Vis Absorption Spectra. As ultraviolet blocking materials, CeO_2 nanocrystals have strong absorption properties in the ultraviolet range. Figure 3a shows the UV/vis absorption spectrum for the hexane colloidal solution of CeO_2 nanocrystals (deep yellow, inset a in Figure 3). There is a strong absorption band below 400 nm in the spectrum, which is due to the charge-transfer transition from O^{2-} (2p) to Ce^{4+} (4f) orbitals in CeO_2.[6a] When CeO_2 nanocrystals were doped with Eu^{3+} ions, we could obtain the CeO_2:Eu^{3+} nanocrystals using the same experimental procedure. Similar to the undoped CeO_2 nanocrystals, the Eu^{3+}-doped CeO_2 nanocrystals can also be dispersed in hexane to form a transparent and light yellow colloidal solution, as shown in inset b of Figure 3. The absorption spectrum of CeO_2:Eu^{3+} nanocrystals (Figure 3b) exhibited a red shift compared with that of CeO_2 nanocrystals. For

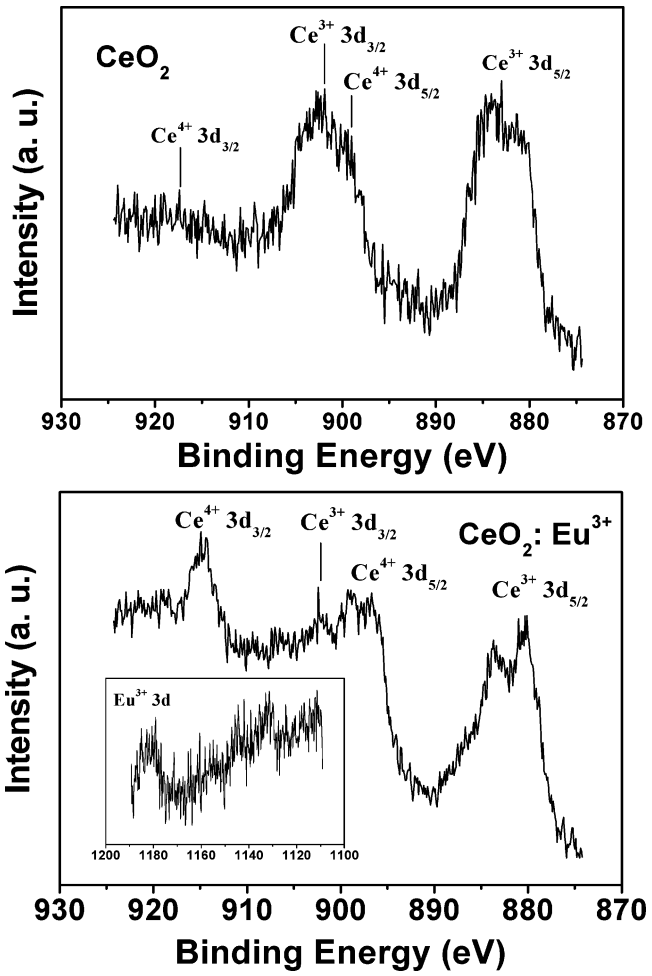

Figure 4. XPS spectra of Ce in CeO_2 (a) and CeO_2:Eu^{3+} (b) nanocrystals. (Inset is the Eu^{3+} 3d peaks in the latter.)

CeO_2 nanocrystals with a particle size of several nanometers, it is well-known that there coexisted a small amount of Ce^{3+} at the surface of CeO_2 and the fraction of Ce^{3+} ions increased with decreasing particle size.[19h,22] The presence of Ce^{3+} ions in the CeO_2 nanocrystals can be confirmed by XPS analysis, as shown in Figure 4 (top).[22] In the XPS spectrum of Ce in CeO_2 nanocrystals, the peaks of Ce^{4+} $3d_{3/2}$ and Ce^{4+} $3d_{5/2}$ at binding energies of 917.2 and 899.0 eV, respectively, are very weak, while those of Ce^{3+} $3d_{3/2}$ and Ce^{3+} $3d_{5/2}$ located at 901.8 and 882.9 eV are relatively strong. This indicates that the Ce^{3+} ions are mainly located on the surface of CeO_2 nanocrystals. Due to the change from Ce^{4+} to Ce^{3+} ions in CeO_2 nanocrystals, the charge-transfer gap between O 2p and Ce 4f bonds increased, which led to the blue-shift of absorption spectrum for CeO_2 nanocrystals compared with CeO_2 bulk powders.[10] As for CeO_2:Eu^{3+} nanocrystals, compared with the undoped CeO_2 nanocrystals, it can be seen from its XPS spectrum (Figure 4, bottom) that the peaks of Ce^{4+} $3d_{3/2}$ and Ce^{4+} $3d_{5/2}$ become strong, while those of Ce^{3+} $3d_{3/2}$ and Ce^{3+} $3d_{5/2}$ are relatively weak. This indicates that the doping of Eu^{3+} ions in the CeO_2 nanocrystals results in the decrease of the Ce^{3+} fraction on the surface due to the replacement of Ce^{3+} by trivalent Eu^{3+} ions. Hence, the red-shifting occurs in the absorption spectrum of CeO_2:Eu^{3+} nanocrystals because of the decrease of the change from Ce^{4+} to Ce^{3+}. Meanwhile, the peaks of Eu^{3+} 3d are present in the XPS spectrum, as shown in Figure 4 (inset), and the presence of Eu element in the CeO_2:Eu^{3+} nanocrystals can also be confirmed by the energy-dispersive X-ray spectrum (Figure S-2). The absorption spectra of CeO_2:Sm^{3+}/Tb^{3+} nanocrystals solutions (Figure S-3) also exhibited a red shift compared with that of CeO_2 nanocrystals; however, the red-shift is not as evident as that of CeO_2:Eu^{3+} nanocrystals.

According to the data for the absorption spectra, the optical band gaps (E_g) of CeO_2 and CeO_2:Eu^{3+} nanocrystals can be estimated by using the following equation:

$$\alpha h\nu = C(h\nu - E_g)^n \quad (1)$$

Here α is the absorption coefficient, $h\nu$ is photon energy, C is the constant, $n = 1/2$ for a directly allowed transition, and $n = 2$ for an indirectly allowed transition.[17] The optical absorption coefficient α was calculated according to the equation $\alpha = (2.303 \times 10^3 A\rho)/lc$, where A is the absorbance of a sample, ρ is the real density of CeO_2 (7.28 g cm^{-3}), l is the path length, and c is the concentration of the ceria suspensions.[12] For direct transitions, the plots of $(\alpha h\nu)^2$ versus photon energy for CeO_2 (a) and CeO_2:Eu^{3+} (b) nanocrystals are shown in Figure S-4. The intersection of the extrapolated linear portions gives the direct band gap energy (E_d), and the values are 3.66 for CeO_2 and 3.33 eV for CeO_2:Eu^{3+} nanocrystals, respectively. For indirect transitions, the plots of $(\alpha h\nu)^{1/2}$ versus photon energy for the above two samples are shown in Figure S-5, and the intersection of the extrapolated linear portions gives the indirect band gap energy (E_i). The E_i values of CeO_2 and CeO_2:Eu^{3+} nanocrystals are 3.13 and 2.69 eV, respectively. The values of E_d and E_i for CeO_2 nanocrystals are consistent with the results reported in the literatures.[17,23] The absorption edge of the present CeO_2 nanocrystals (E_d = 3.66 eV) is blue-shifted evidently compared with that of the bulk CeO_2 powders (E_d = 3.15 eV), which is mainly resulted from quantum confinement effect. The estimated Bohr exciton radius for CeO_2 is about 7−8 nm,[19e] and the average size of our CeO_2 nanocrystals is only around 3.5 nm, which should be small enough for the quantum confinement effect to take place. This effect on the direct band gap (E_d) can be calculated by the following equation:[19i]

$$E_d = E_g + \frac{\hbar^2\pi^2}{2R^2}\left[\frac{1}{m_e} + \frac{1}{m_h}\right] - \frac{1.8e^2}{\epsilon R} \quad (2)$$

Here E_g is the band gap (for CeO_2 powders, E_g = 3.15 eV), R is the radius of the nanoparticles, m_e and m_h are the effective masses of the electron and hole, respectively, and ϵ is the relative dielectric constant of CeO_2 (24.5). Using $m_e = m_h = 0.4m$ (m is the mass of a free electron)[19i] and R = 3.5 nm, the calculated value of E_g is about 3.30 eV, which is less than the E_d value (3.66 eV) of CeO_2 nanocrystals calculated from the absorption spectrum. It is assumed that

(22) Tsunekawa, S.; Fukuda, T.; Kasuya, A. *Surf. Sci.* **2000**, *457*, L437.

(23) Yu, S. H.; Cölfen, H.; Fischer, A. *Colloids Surf., A* **2004**, *243*, 49.

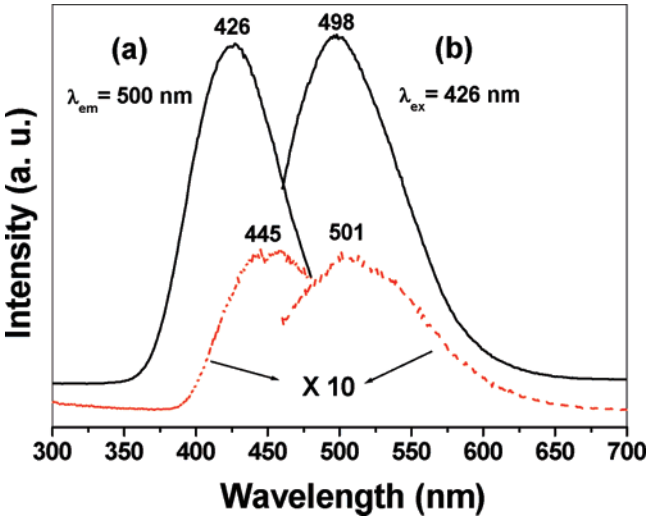

Figure 5. Excitation (a) and emission (b) spectra of CeO_2 (red dash line) and CeO_2:Eu^{3+} (black solid line) nanocrystals in hexane solution.

the valence change from Ce^{4+} to Ce^{3+} on the surface of nanocrystals might have some additional contributions to the blue-shifting of CeO_2 nanocrystals because the change from +4 to +3 increases the charge-transfer gap between O 2p and Ce 4f bands, as reported previously.[10] The presence of Ce^{3+} in CeO_2 nanocrystals has been confirmed by the XPS study mentioned before. When Eu^{3+} ions were doped into CeO_2 nanocrystals, the change from Ce^{4+} to Ce^{3+} ions decreased evidently (by XPS, Figure 4) and the contribution of blue-shifting arising from this valence change became very small. Hence, the E_d (3.33 eV) of CeO_2:Eu^{3+} nanocrystals obtained by UV/vis absorption spectra is very close to the calculated value of E_g (3.30 eV).

Photoluminescence Properties. The photoluminescent (PL) properties of CeO_2 and CeO_2:Eu^{3+} nanocrystals were examined under the identical instrumental conditions. It is shown that CeO_2 nanocrystals exhibit only a very weak broad band emission, which is remarkably enhanced (more than 20 times) by Eu^{3+} doping. Figure 5 gives the excitation (a) and emission (b) spectra for the colloidal solutions of CeO_2 (red dash lines)and CeO_2:Eu^{3+} (black solid lines) nanocrystals. From Figure 5, it can be seen that the excitation and emission spectra (enlarged by 10 times in the figure) for colloidal solution of CeO_2 nanocrystals consist of a broad band with maxima at 445 and 501 nm, respectively, whereas those of CeO_2:Eu^{3+} nanocrystals show much stronger excitation and emission bands with maxima at 426 and 498 nm, respectively. The characteristic f−f emission lines of Eu^{3+} have not been detected in CeO_2:Eu^{3+} nanocrystals. Furthermore, it is surprising that the excitation spectra of CeO_2 and CeO_2:Eu^{3+} nanocrystals are greatly different from their absorption spectra (Figure 3). This indicates that the emissions from CeO_2 and CeO_2:Eu^{3+} nanocrystals are not caused by the charge-transfer transition from O^{2-} to Ce^{4+} but from other emission centers. Basically, we can exclude the possibility that the luminescence is from Ce^{3+} according to the following facts. First, if the emission is from Ce^{3+} due to its 5d−4f transition, the excitation spectrum may be structured due to the transition from 4f ground state to different 5d components split by the crystal fields, and the emissions generally show a double band with an energy difference around 2000 cm^{-1} due to the ground state splitting of Ce^{3+} ($^2F_{5/2}$, $^2F_{7/2}$).[1b] Obviously, these general characteristics for the luminescence of Ce^{3+} have not been observed in the excitation and emission spectra of CeO_2 and CeO_2:Eu^{3+} nanocrystals. Furthermore, if the emission is from Ce^{3+} in CeO_2 and CeO_2:Eu^{3+} nanocrystals, the emission intensity of the former might be stronger than that of the latter because more Ce^{3+} ions may exist in the former than the latter (on the basis of XPS results, Figure 4). But the experimental results do not support this assumption. So we conclude that the luminescence is not from Ce^{3+}.

To explain the above luminescent phenomena, it is necessary to propose a possible luminescence mechanism. As described above, there coexists Ce^{3+} ions on the surface of CeO_2 nanocrystals and the fraction of Ce^{3+} ions increases with decrease of the particle size.[19h,22] Due to the presence of Ce^{3+} ions in CeO_2 nanocrystals, oxygen vacancies are introduced in the crystal to compensate the effective negative charge associated with the trivalent ions.[20b,24−26] The formation of intrinsic oxygen vacancies can be expressed by the following equation:

$$CeO_2 \rightarrow Ce_{1-x}(IV)\cdot Ce_x(III)\cdot O_{2-x/2}\cdot (x/2)Vo^{\bullet\bullet} + (x/4)O_2$$

Here $Vo^{\bullet\bullet}$ is oxygen vacancy. When CeO_2 nanocrystals are doped with Eu^{3+} ions, extrinsic oxygen vacancies ($Vo^{\bullet\bullet}$) will be generated in the fluorite lattice of the nanocrystals and the fraction of trivalent Ce^{3+} ions in the doped nanocrystals must be decreased due to the replacement of Ce^{3+} by trivalent Eu^{3+} ions. The decreasing of Ce^{3+} ions and the presence of Eu^{3+} ions on the surface of CeO_2:Eu^{3+} nanocrystals have been confirmed by XPS, EDS analysis, and absorption spectra data. The reaction equation can be expressed as

$$CeO_2 \rightarrow Ce_{1-y}(IV)\cdot Ln_y(III)\cdot O_{2-y/2}\cdot (y/2)Vo^{\bullet\bullet} + (y/4)O_2$$

where Ln is a trivalent lanthanide ion (e.g., Eu^{3+}). The $Vo^{\bullet\bullet}$ concentration in CeO_2:Eu^{3+} nanocrystals must be higher than that in the undoped CeO_2 nanocrystals because the doping concentration of Eu^{3+} is much larger than the fraction of Ce^{3+} in undoped nanocrystals. Considering that the PL intensity of the CeO_2:Eu^{3+} nanocrystals is so strong while that of CeO_2 nanocrystals is very weak (Figure 5), we can safely deduce that the strong emission of CeO_2:Eu^{3+} nanocrystals excited at 440 nm may arise from the presence of a large amount of $Vo^{\bullet\bullet}$ in the doped nanocrystals.

The assumed photoluminescence mechanism can be illustrated by the schematic diagram of the energy band of

(24) McBride, J. R.; Hass, K. C.; Poindexter, B. D.; Weber, W. H. *J. Appl. Phys.* **1994**, *76*, 2435.
(25) Li, L. P.; Li, G. S.; Che, Y. L.; Su, W. H. *Chem. Mater.* **2000**, *12*, 2567.
(26) (a) Dutta, P.; Pal, S.; Seehra, M. S.; Shi, Y.; Eyring, E. M.; Ernst, R. D. *Chem. Mater.* **2006**, *18*, 5144. (b) Verma, A.; Karar, N.; Bakhshi, A. K.; Chander, H.; Shivaprasad, S. M.; Agnihotry, S. A. *J. Nanopart. Res.* **2007**, *9*, 317. (c) Ou, D. R.; Mori, T.; Ye, F.; Kobayashi, T.; Zou, J.; Auchterlonie, G.; Drennan, J. *Appl. Phys. Lett.* **2006**, *89*, 171911.

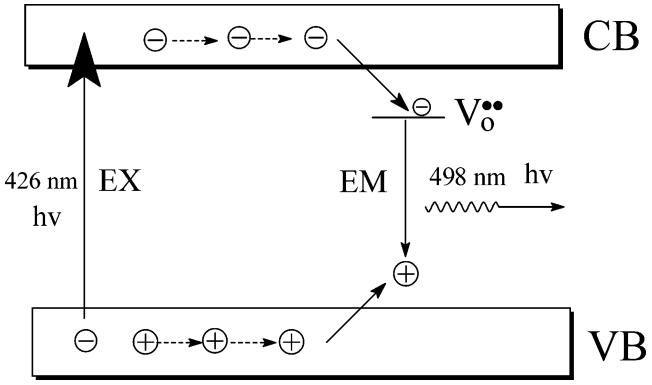

Figure 6. Schematic diagram for the luminescence process in CeO_2:Eu^{3+} nanocrystals. The conduction band (CB), valence band (VB), oxygen vacancy ($V_O^{\bullet\bullet}$), electron (⊖), and hole (⊕) are shown inside the figure.

CeO_2:Eu^{3+} nanocrystals, as shown in Figure 6.[27] The excitation band peaking at 426 nm (2.93 eV) can be basically attributed to the indirectly allowed transition (the calculated value of E_i is about 2.70 eV). Upon excitation with the light of 426 nm, electrons were excited from the valence band (VB) to the conduction band (CB), producing holes in VB. The electrons in CB move freely and are trapped by the oxygen vacancy ($V_O^{\bullet\bullet}$) to form the donor; meanwhile the holes may populate above the VB to form the acceptor. The recombination of the electrons and holes thus produces the visible emission around 500 nm. If the oxygen vacancy ($Vo^{\bullet\bullet}$) in CeO_2:Eu^{3+} nanocrystals is the key factor to lead to the visible emission band, then CeO_2 nanocrystals doped with other trivalent lanthanide ions should produce a similar emission band. So we synthesized Sm^{3+}- and Tb^{3+}-doped CeO_2 nanocrystals and measured their PL spectra. Figure S-6 shows the PL spectra of CeO_2:Sm^{3+} and CeO_2:Tb^{3+} nanocrystal solutions, respectively. It can be seen that the excitation and emission spectra of Sm^{3+}- and Tb^{3+}-doped CeO_2 nanocrystals are similar to that of CeO_2:Eu^{3+} nanocrystals. This further confirms that the emission band (∼500 nm) is not the characteristic emission of doping lanthanide ions and must be relative to the oxygen vacancy in CeO_2 nanocrystals.

Finally, we explain the absence of Eu^{3+} emission in CeO_2 nanocrystals briefly. We think there are several possibilities that may bring about the absence of Eu^{3+} emission in CeO_2 nanocrystals. One possible reason is that the Eu^{3+} ions are located at O_h centrosymmetric sites (Ce^{4+} in CeO_2) in which the radiative transition probability of Eu^{3+} is very small. Other reasons include the formation of $Eu^{2+}-Ce^{4+}$ ion pairs, which are not luminescent.[28] Furthermore, the absorption of UV energy occurred in CeO_2 very easily compared to the $Eu^{3+}-O^{2-}$ charge transfer and f−f transitions of Eu^{3+}, but the absorbed energy is unable to transfer to Eu^{3+}. All these factors can quench the emission of Eu^{3+} in CeO_2 nanocrystals.

Conclusions

We have synthesized the CeO_2 nanocrystals doped and undoped with trivalent lanthanide ions (Eu^{3+}, Sm^{3+}, Tb^{3+}) and discussed their optical properties. The as-prepared CeO_2 and CeO_2:Eu^{3+} (Sm^{3+}, Tb^{3+}) nanocrystals are highly uniform and can be dispersed in hexane to form a transparent colloidal solution. The absorption spectrum of CeO_2:Eu^{3+} nanocrystals exhibits a red shift with respect to that of undoped CeO_2 nanocrystals; i.e., the blocking range for UV is enhanced by doping lanthanide ions in CeO_2 nanocrystals. The CeO_2:Eu^{3+} nanocrystals show a remarkable enhanced PL intensity with respect to the CeO_2 nanocrystals due to the increase of oxygen vacancy in the CeO_2 nanocrystals.

Acknowledgment. This project is financially supported by the Foundation of "Bairen Jihua" of the Chinese Academy of Sciences, the MOST of China (Grant 2003CB314707), and the National Natural Science Foundation of China (Grants NSFC 50572103, 20431030, 00610227).

Supporting Information Available: Figures S1 (particle size distribution histogram for CeO_2 nanocrystals), S2 (EDS of CeO_2:Eu^{3+} nanocrystals), S3 (UV/vis absorption spectra), S4 and S5 (plots of $(\alpha h\nu)^2$ and $(\alpha h\nu)^{1/2}$ versus photon energy for CeO_2 and CeO_2:Eu^{3+} nanocrystals), and S6 (excitation and emission spectra of CeO_2:Sm^{3+} and CeO_2:Tb^{3+} nanocrystals). This material is available free of charge via the Internet at http://pubs.acs.org.

IC0701256

(27) Yang, J.; Lin, C. K.; Wang, Z. L.; Lin, J. *Inorg. Chem.* **2006**, *45*, 8973.
(28) Blasse, G.; Bril, A. *J. Chem. Phys.* **1967**, *47*, 1920.